Photoionization cross section of Si II from threshold to 1 keV*

Gaelen R. Daum and Hugh P. Kelly
Physics Department, University of Virginia, Charlottesville, Virginia 22901
(Received 7 July 1975)

The techniques of many-body perturbation theory with interacting resonances are used to calculate the photoionization cross section of Si II from threshold to 1 keV. The Rayleigh-Schrödinger expansion with *LS* coupled states and the Brueckner-Goldstone expansion are compared. Correlations among the $2p$, $3s$, and $3p$ electrons are shown to have a large effect on the cross section. Resonances from $3s3p\,np$, $2p^5 3s^2 3p\,ns$, $2p^5 3s^2 3p\,nd$, and $2s2p^6 3s^2 3p\,np$ configurations are included.

I. INTRODUCTION

The astrophysical importance of period-II and -III elements is well known.[1,2] Knowledge of their oscillator strengths and photoionization cross sections are necessary for calculation of stellar abundances, opacity, electron density and other properties.[3] Experimental determination of the photoionization cross section of an ion such as Si II is quite difficult because of recombination effects, and calculations including electron correlations have not yet been performed.

This work utilizes the techniques of many-body perturbation theory to calculate the photoionization cross section of Si II from threshold to 1 keV, including resonances from autoionizing states. Both the Brueckner-Goldstone[4] perturbation expansion and the Rayleigh-Schrödinger perturbation expansion were utilized in the calculation. The connection between these two approaches is discussed in Sec. II.

The electronic configuration of the Si II ground state is $1s^2 2s^2 2p^6 3s^2 3p\ ^2P^o$. Dipole transitions to the following final states were considered: $1s^2 2s^2 2p^6 3s^2\ (^1S)\,ks\ ^2S$; $1s^2 2s^2 2p^6 3s^2\ (^1S)\,kd\ ^2D$; $1s^2 2s^2 2p^6 3s\,3p\ (^3P)\,kp\ ^2S$, ^2P, and ^2D; $1s^2 2s^2 2p^6 3s\,3p\ (^1P)\,kp\ ^2S$, ^2P and ^2D; $1s^2 2s^2 2p^5\,ks\ (^1P)\,3s^2 3p\ ^2S$, ^2P, and ^2D; and $1s^2 2s^2 2p^5\,kd\ (^1P)\,3s^2 3p\ ^2S$, ^2P, and ^2D, where kl represents the photoelectron of energy $\frac{1}{2}k^2$ and orbital angular momentum l. The choice of coupling schemes is discussed in Sec. III. Correlations among the $2p$, $3s$, and $3p$ subshells were included.

II. THEORY

The application of many-body perturbation theory to photoionization processes, including the interaction of resonances due to autoionizing states,[4,5] was recently presented.[6] This paper will follow the notation and development given there, and the reader is referred to Ref. 6 for a detailed discussion.

The basic relation[5] is

$$\sigma(\omega) = 4\pi(\omega/c)\,\mathrm{Im}\,\alpha(\omega), \tag{1}$$

where $\alpha(\omega)$, the frequency-dependent dipole polarizability, has a well-defined perturbation expansion,[7] and c is the speed of light. (Atomic units are used throughout unless otherwise noted.) As shown previously,[8] Eq. (1) becomes

$$\sigma(\omega) = 8\pi(\omega/ck)\,N|Z(p\to k)|^2, \tag{2}$$

where

$$Z(p\to k) = \langle\Psi_k|\sum_i z_i|\Psi_0\rangle \tag{3}$$

is the length form of the electric dipole matrix element, and Ψ_0 and Ψ_k are exact many-particle ground and continuum states. The notation $Z(p\to k)$ is used to stress that the dominant contribution from the exact many-particle states is from matrix elements where a spin-orbital p of the initial determinant undergoes a dipole transition to a spin-orbital k of the final determinant. The normalization factor N is usually close to one and arises because $|\Psi_0\rangle$ is not normalized to unity[9]; and $k = (2[\omega - I])^{1/2}$, I being the ionization energy. There is included a factor $2/k$ in Eq. (2) due to the form of the continuum orbitals and taking the imaginary part indicated in Eq. (1). The continuum orbitals are normalized such that

$$R_k(r)\to(1/r)\cos[kr + (q/k)\ln(2kr) - \tfrac{1}{2}\pi(l-1) + \delta_l] \tag{4}$$

as $r\to\infty$, where $V(r)\to q/r$. The energy of a continuum orbital of this form is $E_k = \frac{1}{2}k^2$ in atomic units, and sums over continuum orbitals are evaluated by

$$\sum_k \to \frac{2}{\pi}\int dk.$$

The velocity form of the cross section may be obtained by using the identity[10]

$$\langle\Psi_k|\sum_i z_i|\Psi_0\rangle = -(E_k - E_0)^{-1}\langle\Psi_k|\sum_i \nabla_{zi}|\Psi_0\rangle\,, \qquad (5)$$

where E_k and E_0 are the energy eigenvalues of $|\Psi_k\rangle$ and $|\Psi_0\rangle$, respectively.

The matrix element $Z(p \to k)$ is obtained from the series of all open many-body diagrams with one dipole interaction and any number of correlation interactions.[7] In this work we calculated diagrams which appear in the random-phase approximation with exchange (RPAE). Other diagrams which should be included in the RPAE for an open-shell atom were also included, as well as normalization diagrams.[9]

Some typical diagrams are shown in Figs. 1(a)–1(c). Solid dots represent dipole interactions; other dashed lines represent Coulomb interactions; and time increases upwards. Figure 1(a) is the lowest-order diagram, representing a dipole transition from a ground-state orbital p to an excited-state orbital k. Figures 1(b) and 1(c) and their exchanges represent terms with one Coulomb interaction. When the Coulomb interaction occurs after the dipole interaction, as in Fig. 1(b), it is a final-state correlation diagram. In Fig. 1(c) the Coulomb interaction occurs before the dipole interaction,

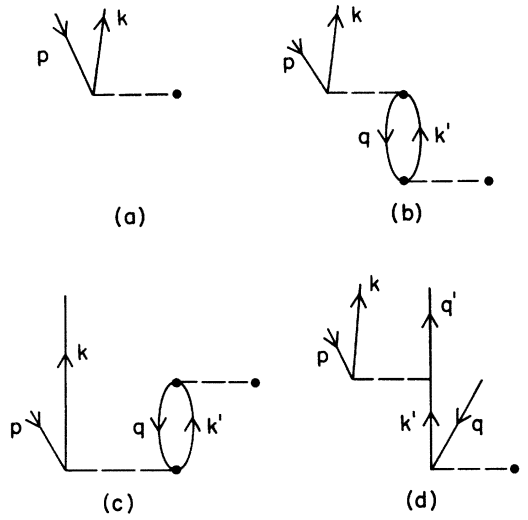

FIG. 1. Diagrams contributing to $Z(p \to k)$. (a) Lowest-order, dipole matrix element; (b) final-state correlation diagram, first order in Coulomb interaction; (c) ground-state correlation diagram, first order in Coulomb interaction; (d) final-state correlation diagram occurring for open-shell atoms. Orbitals of the open-shell occupied in the ground state are labelled q; orbitals of the open-shell not occupied in the ground state labelled q'. Exchange diagrams are not shown but were included in the calculation.

and it is a ground-state correlation diagram. Figures 1(a)–1(c) depict processes where the final state differs from the ground state by one spin orbital.

It is also possible to have processes where the final state differs from the ground state by more than one spin orbital, and this may correspond to photoionization with excitation. An example in Si II is Fig. 1(d) with $p = 3s$, $k = kp$, $q = 3p$ occupied in the ground state, $k' = ks$ and kd, and $q' = np$ ($n \geq 4$). In an open-shell atom, it is also possible to have an excited-state orbital and a ground-state orbital with the same n and l but different m_l and m_s. Figure 1(d), with $p = 3s$, $k = kp$, $k' = ks$ and kd, $q = 3p$ occupied in the ground state, and $q' = 3p$ not occupied in the ground state, is an example of this. In this case, Fig. 1(d) has the same radial part as Fig. 1(b) with $p = 3s$, $k = kp$, $q = 3p$ occupied in the ground state, and $k' = ks$ and kd; in this case Fig. 1(d) does not correspond to photoionization plus excitation. In the Brueckner-Goldstone expansion, only the diagrams of Fig. 1(b) would normally be included. It is found however, that the diagrams of Fig. 1(d) are necessary to extract from the Brueckner-Goldstone expansion contributions to particular LS terms. This is discussed in more detail later in this section.

Denominators occurring after the dipole interaction are shifted by $+\omega$. When the denominator vanishes, a small imaginary part $i\eta$ is added, and the denominator is treated according to

$$\lim_{\eta \to 0} (D + i\eta)^{-1} = \mathrm{P}D - i\pi\delta(D), \qquad (6)$$

where P denotes a principal-value integration. The $-i\pi\delta(D)$ contributions are denoted on the diagrams by a horizontal line. For example, Fig. 1(b) represents

$$\frac{2}{\pi}\int dk'\,\langle kq|v|pk'\rangle(E_q - E_{k'} + \omega + i\eta)^{-1}\langle k'|z|q\rangle\,, \qquad (7)$$

where E_q and $E_{k'}$ are the single-particle energies of states q and k', and v is the Coulomb interaction.

Configurations containing excited bound states which are degenerate in energy with the photoionization continuum lead to resonances and are referred to as resonance configurations. Figure 1(b) is the lowest-order resonance diagram, representing resonance effects provided that the configuration with hole q and particle k' (with k' bound) is a resonance configuration.

To calculate $Z(p \to k)$, we first note that it is possible to factor the angular coefficient of Fig. 1(a) from each of the diagrams. The sum of the resulting series of reduced diagrams is denoted

TABLE I. Contributions from Figs. 1(b) and 1(d) to $\langle 3s3p\,(^{1,3}P)kp\,{}^2S,\ {}^2P,\ {}^2D|\sum v_{ij}|3s^2 k s\,{}^2S\rangle\langle 3s^2 ks\,{}^2S|\sum z_i|3s^2 3p\,{}^2P^o\rangle$.

Figure	Orbitals[a] p	k	q'	Angular part of diagram	Projections onto final LS-coupled states $(^3P)kp\,{}^2S$	$(^1P)kp\,{}^2S$	$(^3P)kp\,{}^2P$	$(^1P)kp\,{}^2P$	$(^3P)kp\,{}^2D$	$(^1P)kp\,{}^2D$
1b	0^+	0^+		$1/3\sqrt{3}$	$1/3\sqrt{2}$	$1/\sqrt{6}$	0	0	$-\frac{1}{3}$	$-1/\sqrt{3}$
1b	0^-	0^-		$1/3\sqrt{3}$	$2/3\sqrt{2}$	0	0	0	$-\frac{2}{3}$	0
1d	0^+	1^+	-1^+	$-1/3\sqrt{3}$	$-1/3\sqrt{2}$	$-1/\sqrt{6}$	$1/2\sqrt{3}$	$\frac{1}{2}$	$-\frac{1}{6}$	$-1/2\sqrt{3}$
1d	0^-	1^-	-1^+	$-1/3\sqrt{3}$	$-2/3\sqrt{2}$	0	$-1/\sqrt{3}$	0	$-\frac{1}{3}$	0
1d	0^+	-1^+	1^+	$-1/3\sqrt{3}$	$-1/3\sqrt{2}$	$-1/\sqrt{6}$	$-1/2\sqrt{3}$	$-\frac{1}{2}$	$-\frac{1}{6}$	$-1/2\sqrt{3}$
1d	0^-	-1^-	1^+	$-1/3\sqrt{3}$	$-2/3\sqrt{2}$	0	$\frac{1}{3}$	0	$-\frac{1}{3}$	0

[a] The labels are $p = 3s$, $k = kp$, $q = 3p$ occupied in the ground state, $q' = 3p$ not occupied in the ground state, and k' = excited s orbital. The notation 1^- in the column under k refers, then, to continuum orbital with $l = 1$, $m_l = 1$, and $m_s = -\frac{1}{2}$. The ground-state determinant is $(3s0^+,\ 3s0^-,\ 3p0^+)$ so q, k' have $m_l = 0$, $m_s = \frac{1}{2}$.

by $Z_R(p \to k)$, which is usually complex.[6] For Si II it is found that $Z_R(p \to k)$ is independent of the m_l of the orbital p and also of M_L, the total for the final state.

In previous work[6] it was found that diagrams such as Fig. 1(b), with k' an excited bound orbital nl, were resonance diagrams for all n not occupied in the ground state. It was convenient to consider $Z_R(p \to k)$ to be the sum of a nonresonant part $Z_R^D(p \to k)$ which involved only excitations of q to the continuum and a resonant part D_{RT} which involved only excitations of q to excited bound states. For an open-shell atom, it may not be true that Fig. 1(b) with $k' = nl$ is a resonance diagram for all n. In Si II, for example, Fig. 1(b) with $p = 3p$ occupied in the ground state, $k = kd$ or ks, $q = 3s$, and $k' = 3p$ not occupied in the ground state, is not a resonance diagram since the $3s\,3p^2$ configuration lies below threshold. In this case, it is convenient to consider $Z_R(p \to k)$ to be the sum of $Z_R^D(p \to k)$ and D_{RT} as defined above, but $Z_R^D(p \to k)$ is no longer the total nonresonant cross section since those nonresonant diagrams involving excitations of q to excited bound states are included in D_{RT}.

Calculation of $Z_R^D(p \to k)$ may utilize either the Rayleigh-Schrödinger (RS) expansion with LS-coupled, multideterminant states or the Brueckner-Goldstone (BG) expansion which effectively uses single-determinant states. Which method is simpler to use at any point in the calculation depends upon the configuration and coupling schemes involved. Both are found to yield identical results, as they must, since the two representations of the states are related through a unitary transformation, and both expansions use the same perturbation. An illustration of the connection between the two approaches is seen by considering Figs. 1(b) and 1(d), plus exchange, with $p = 3s$, $k = kp$, $q = 3p$ occupied in the ground state, $q' = 3p$ not occupied in the ground state, and $k' = ns$. The orbital kl represents a continuum electron with orbital angular momentum l, and ns represents either a bound or continuum orbital with $l = 0$. We take the ground state of the atom to be the determinant $(3s0^+, 3s0^-, 3p0^+)$. Other closed shells are not indicated. The results of the BG expansion are summarized in Table I. The projections are obtained by projecting the final, single-determinant state indicated by the diagram onto the LS-coupled, multideterminant state. The net result for all the diagrams of Table I and the corresponding exchange diagrams is $[-\frac{2}{3}{}^{1/2}R^1(3p, kp; 3s, ns) + \frac{1}{6}{}^{1/2}R^1(kp, 3p; 3s, ns)] \times \langle ns|z|3p\rangle$ for the final state $3s\,3p(^1P)kp\,{}^2S$, and $\frac{1}{2}R^1(kp, 3p; 3s, ns)\langle ns|z|3p\rangle$ for the final state $3s\,3p(^3P)kp\,{}^2S$. All other contributions are zero. Note that the angular part of the dipole matrix element has not been included in the expressions above, but is included in Table I. This angular factor is $\frac{1}{3}{}^{1/2}$.

In terms of the RS expansion, we start with a $3s^2\,3p\,{}^2P^o$ ground state and go to a $3s^2 k's$ intermediate configuration via the dipole interaction. This interaction must leave the $3s\,3p\,kp$ final configuration in a ^2S state. The contributions to ^2P and ^2D final states are zero, and we must evaluate only the matrix elements

$$\langle 3s\,3p(^{1,3}P)kp\,{}^2S|\sum_{i<j} v_{ij}|3s^2 k's\,{}^2S\rangle \times \langle 3s^2 k's\,{}^2S|\sum_i z_i|3s^2\,3p\,{}^2P^o\rangle ,$$

which yields the same result as the BG expression.

In performing calculations with the BG expansion, only the diagrams of Fig. 1(b) would be included if we only are calculating $\sigma(\omega)$ correct to first order in the correlations. As shown above, however, we must include the diagrams of Fig. 1(d) if we wish to extract contributions to particu-

lar LS terms. Note that the contributions to the total photoionization cross section are the same in both cases.

The chief task in the BG expansion is to list the diagrams representing all possible contractions of annihilation and creation operators for each order of the perturbation. The chief task in the RS expansion is the LS coupling of all possible configurations. The angular parts of the Coulomb and dipole matrix elements are also more difficult to evaluate with multideterminant states. In this calculation, it was generally found more convenient to evaluate final-state correlations with the BG expansion. A more detailed comparison of these methods is given in a forthcoming paper.[11]

Consider the diagram of Fig. 1(b) with k' an excited bound orbital nl. If $E_q - E_{nl} - E_p < 0$, then the configuration with hole q and particle nl is a resonance configuration, and Fig. 1(b) is the lowest-order resonance diagram, which we will call RDI. When the single-particle states nl have two possible angular momenta, we have the diagram of Fig. 1(b) corresponding to each of the possible values. An example in Si II is Fig. 1(b) with $p = 3s$, $k = kp$, $q = 2p$, and $nl = ns$ or nd. In higher orders of the perturbation expansion we have diagrams similar to RDI, but with the segments shown in Figs. 2(c) and 2(d) repeated. Then RDI and these higher-order diagrams form two geometric series (corresponding to the two possible values of l in the $q \to nl$ transition), each with the ratio

$$R_G = -i \sum_{n,l} \frac{\frac{1}{2}\Gamma_{nl}(l;\omega)}{D_n(l;\omega)}, \tag{8}$$

where

$$\tfrac{1}{2}\Gamma_{nl}(l;\omega) = \frac{2}{k}\left|\langle \Phi_k | \sum v_{ij} | \Phi_{nl}\rangle\right|^2 \tag{9}$$

is the half-width of the nth resonance of the series $q \to nl$, and

$$D_{nl}(l;\omega) = E_q - E_{nl} + \omega. \tag{10}$$

In the BG expansion, $|\Phi_k\rangle$ is the determinant formed by replacing p with k in $|\Phi_0\rangle$ (the ground state) and $|\Phi_{nl}\rangle$ the determinant formed by replacing q with nl in $|\Phi_0\rangle$. In the RS expansion, the many-particle states of the intermediate configuration with hole q and particle nl may contribute to several different LS terms. This is analogous to the BG treatment above, except that the sum over l becomes a sum over the LS couplings. Also, $|\Phi_k\rangle$ and $|\Phi_{nl}\rangle$ are multideterminantal states rather than single determinants, and the single-particle energies in Eq. (10) are replaced by the energies of the states $|\Phi_k\rangle$ and $|\Phi_{nl}\rangle$. The sum of the geometric series is then $\mathrm{RDI}(q \to nl)(1 - R_G)^{-1}$, where $\mathrm{RDI}(q \to nl)$ is used to stress that there is an RDI corresponding to each possible l or each possible LS term.

We include in RDI correlation modifications of the basic $q \to nl$ dipole matrix element $Z^D(q \to nl)$. The angular coefficient of the lowest-order diagram may be factored from each diagram of $Z^D(q \to nl)$. As was found for $Z_R(p \to k)$, $Z_R^D(q \to nl)$ may be complex.[6] Figures 1(a)–1(c), with the labels for the p and q hole lines and the k and k' particle lines interchanged, are diagrams which contribute to $\mathrm{Re}Z^D(q \to nl)$. Figure 1(b) with the labels p, q, and k, $k' = nl$ interchanged and the denominator treated according to $-i\pi\delta(D)$ is the lowest-order contribution to $\mathrm{Im}Z^D(q \to nl)$.

The contribution to $Z_R(p \to k)$ from Fig. 1(b) where the $q \to nl$ dipole matrix element is replaced by $\mathrm{Re}Z^D(q \to nl)$ may be written

$$D_{RT1} = \left(\sum_{l,n} \frac{q_{nl}(l)\frac{1}{2}\Gamma_{nl}(l;\omega)}{D_{nl}(l;\omega)}\right) Z_R^D(p \to k) \equiv \sum_{l,n} Q_{nl}(l;\omega) Z_R^D(p \to k), \tag{11}$$

where

$$q_{nl}(l) \equiv \mathrm{Re}Z^D(q \to nl) \times \left[(2/k)\langle \Phi_k | \sum v_{ij} | \Phi_{nl}\rangle Z^D(p \to k)\right]^{-1}; \tag{12}$$

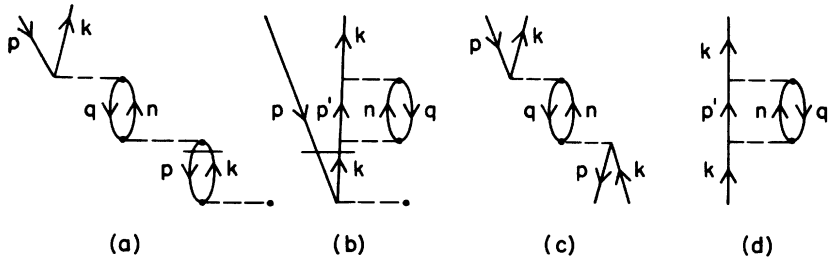

FIG. 2. Important higher-order diagrams contributing to $Z(p \to k)$. (a) final-state correlation diagram; (b) final-state correlation diagram which occurs when p and p' refer to orbitals of an open shell, p being occupied in the ground state and p' being unoccupied in the ground state; (c) and (d) are segments of (a) and (b), respectively, which are repeated in higher-order diagrams.

TABLE II. Ionization potentials used in this calculation.

Orbital	Energy (a.u.) [a]
$2s$	7.052 298
$2p$	4.104 736
$2s$ (^1P core)	0.978 196
$3s$ (^3P core)	0.840 944
$3p$	0.601 052

[a] The sources of the energies are given in Sec. III.

note that $Z^D(p \to k)$ in Eq. (12) is not reduced, i.e., it contains the over-all angular coefficient that was previously factored out.

The contributions to $Z_R(p \to k)$ from Fig. 1(b) when the $q \to nl$ dipole matrix element is replaced by $\mathrm{Im}Z^D(q \to nl)$ may be written

$$D_{RT2} = -i\left(\sum_{l,n} \frac{\frac{1}{2}\Gamma_n(l;\omega)}{D_{nl}(l;\omega)}\right) Z_R^D(p \to k). \tag{13}$$

The lowest-order contribution to D_{RT2} is seen in Figs. 2(a) and 2(b) with p an open-shell orbital occupied in the ground state and p' an open-shell orbital not occupied in the ground state, but in the same subshell as p. In higher orders of the perturbation expansion we find diagrams similar to Figs. 2(a) and 2(b) but with the segments above the horizontal line [shown in Figs. 2(c) and 2(d)] repeated. Figures 2(a) and 2(b) and these higher-order diagrams also form a geometric series with ratio given by Eq. (8).

Summing the series whose first term is D_{RT1} and adding the sum of the series whose first term is D_{RT2}, we obtain D_{RT}, our contribution to $Z_R(p \to k)$ from diagrams involving excited bound states:

$$D_{RT} = (D_{RT1} + D_{RT2})(1 - R_G)^{-1}. \tag{14}$$

Other diagrams involving bound resonance configurations are possible, but we expect them to be less important than those included in this work.

Combining D_{RT} with $Z_R^D(p \to k)$ yields

$$Z_R(p \to k) = (1 - R_G)^{-1}\left(1 + \sum_{l,n} Q_{nl}(l;\omega)\right) Z_R^D(p \to k), \tag{15}$$

where $Q_{nl}(l;\omega)$ is defined by Eq. (11). This expression for $Z_R(p \to k)$ is the analog of Eq. (23) of Ref. 6 for the case of more than one series of interacting resonances. Unless the series overlap such that the separation between resonances is not small compared to the half-width of either, the effect of interacting resonances on the cross section is slight. An example where good agreement with experiment is obtained without including interactions among resonances is given in Ref. 15. A case where interacting resonances were found to be very important is presented in Ref. 6.

III. CALCULATIONS

In the evaluation of diagrams, sums over bound states are done explicitly for $n \leq 12$ and the n^{-3} rule[9] is used to sum from $12 < n \leq \infty$. Sums over continuum states and the normalization of the continuum orbitals have been discussed in Sec. II.

When using the BG expansion, the final states are not necessarily LS coupled. It is possible to factor the m_l dependence of the diagrammatic series and average over the initial states. The RS expansion, however, allows many LS terms to arise from the same final configuration, and one averages over M_L for each possible L and then adds the cross sections.

Experimental energies were used in the energy denominators wherever possible. This is equivalent to including certain higher-order correlation diagrams which shift the HF single-particle energy.[7,12] The $3p$ and $3s$ removal energies were taken from Moore.[16] Two $3s$ removal energies were used, corresponding to leaving the residual Si III in a ^1P and a ^3P state. The $2p$ removal energy was

TABLE III. Some values of the $3p$ subshell cross section σ (10^{-18} cm^2).

	Length		Velocity	
ω (eV)	Uncorrelated	Correlated	Uncorrelated	Correlated
16.5682	1.249 723	1.086 394	0.947 568	1.289 227
26.7726	0.180 299	0.290 607	0.161 526	0.314 777
46.9687	0.212 417	0.269 306	0.179 751	0.281 675
70.7789	0.156 145	0.166 876	0.130 882	0.179 587
138.8080	0.052 961	0.048 164	0.045 114	0.048 444
234.0488	0.017 427	0.020 001	0.014 972	0.017 549
356.5012	$6.347\,09\times10^{-3}$	7.379×10^{-3}	$5.487\,67\times10^{-3}$	6.3289×10^{-3}
506.1653	$2.539\,10\times10^{-3}$	2.914×10^{-3}	$2.222\,70\times10^{-3}$	$2.524\,45\times10^{-3}$
683.0411	$1.096\,39\times10^{-3}$	1.224×10^{-3}	$9.773\,09\times10^{-4}$	$1.093\,78\times10^{-3}$
887.1285	$5.052\,10\times10^{-4}$	5.72×10^{-4}	$4.595\,44\times10^{-4}$	$5.245\,97\times10^{-4}$

TABLE IV. Some values of the 3s subshell cross section ($3s3p\,^3P$ core) σ (10^{-18}cm^2).

	Length		Velocity	
ω (eV)	Uncorrelated	Correlated	Uncorrelated	Correlated
23.0961	0.367 913	0.291 192	0.267 227	0.393 730
30.5368	0.366 796	0.377 226	0.301 624	0.462 497
53.4966	0.230 629	0.272 758	0.214 639	0.335 181
107.9199	0.092 364	0.134 198	0.089 513	0.157 374
189.5548	0.039 611	0.053 579	0.037 512	0.057 183
240.5767	0.027 060	0.032 134	0.025 238	0.035 992
363.0291	0.013 5146	0.016 6648	0.012 320	0.016 888
512.6932	$7.227\,50\times10^{-3}$	$9.303\,07\times10^{-3}$	$6.526\,23\times10^{-3}$	$8.680\,45\times10^{-3}$
689.5689	$4.067\,72\times10^{-3}$	$5.434\,11\times10^{-3}$	$3.675\,68\times10^{-3}$	$4.827\,49\times10^{-3}$
893.6563	$2.386\,36\times10^{-3}$	$3.279\,90\times10^{-3}$	$2.170\,03\times10^{-3}$	$2.876\,20\times10^{-3}$

obtained by comparing $E_{\rm HF}(2p^6\,3s^2\,3p^2)$-$E_{\rm HF}(2p^5\,3s^2\,3p^2)$ for Si I with the ESCA[17] value for the $2p$ removal energy in Si I. The HF value using the center of gravity of the configurations was approximately 10 eV too high. Assuming the $3s$ and $3p$ electrons to be of comparable importance to the correlation energy, we calculated $E_{\rm HF}(2p^6\,3s^2\,3p)$-$E_{\rm HF}(2p^5\,3s^2\,3p)$ for the center of gravity of the configurations in Si II and reduced the result by 7.5 eV to approximate correlation effects. The $2s$ removal energy was taken to be the HF $2s$ single-particle energy. The values of the ionization energies are given in Table II.

Both length and velocity forms of the cross section were calculated. The total cross sections for each subshell agree to within 30% for the two forms, the largest differences occurring near threshold. Differences away from threshold are usually within 10–15%. Some representative values of the length and velocity subshell cross sections are presented in Tables III–VI. An interesting result of using LS-coupled wave functions is that adding correlations to the dipole matrix element affects the agreement between length and velocity forms to different degrees, depending upon the particular LS state of the configuration. An example is the case of correlations for the $3s$ subshell. One of the largest diagrams is Fig. 1(b) with $p=3s$, $k=kp$, $q=3p$ and $k'=ks$ or kd. Possible final states are $3s\,3p(^{1,3}P)kp\,^2S$, ^2P, and ^2D, but this diagram has no projection onto the ^2P state since the $q\to k'$ excitation can only result in ^2S or ^2D. Thus, the ^2P cross section is unaffected while the ^2S and ^2D cross sections both have large correlations due to this diagram. Any discrepancy between the length and velocity forms of this diagram will be reflected in the ^2S and ^2D cross sections but not in the ^2P cross section.

Ground- and final-state correlations among the $2p$, $3s$, and $3p$ subshells were included in Z_R^D to first order in the Coulomb interaction for all subshells. The coupling schemes for particular cases are discussed below.

A. $3p$ subshell cross section

The excitation of the $3p$ electron in Si II can only lead to ^2S and ^2D final states, corresponding to $3p\to ks$ and $3p\to kd$ transitions, respectively. The $3p$ ground-state orbital was calculated in the Hartree-Fock ground-state potential. The continuum s and d states were calculated in a V^{N-1} potential[7]

TABLE V. Some values of the 3s subshell cross section ($3s\,3p\,^1P$ core) σ (10^{-18} cm^2).

	Length		Velocity	
ω (eV)	Uncorrelated	Correlated	Uncorrelated	Correlated
26.8309	0.142 487	0.308 267	0.076 686	0.231 915
34.2716	0.137 219	0.185 784	0.089 585	0.163 702
57.2314	0.082 244	0.064 202	0.066 877	0.079 817
81.0416	0.051 180	0.039 942	0.044 832	0.054 977
149.0708	0.020 379	0.028 210	0.018 614	0.033 338
244.3115	$9.160\,06\times10^{-3}$	0.015 233	$8.284\,04\times10^{-3}$	0.016 611
366.7640	$4.551\,22\times10^{-3}$	$6.985\,49\times10^{-3}$	$4.064\,74\times10^{-3}$	$7.488\,43\times10^{-3}$
516.4281	$2.426\,72\times10^{-3}$	$3.559\,35\times10^{-3}$	$2.159\,68\times10^{-3}$	$3.729\,08\times10^{-3}$
693.3038	$1.363\,25\times10^{-3}$	$2.034\,43\times10^{-3}$	$1.218\,63\times10^{-3}$	$2.091\,98\times10^{-3}$
897.3912	$7.987\,79\times10^{-4}$	$1.312\,23\times10^{-3}$	$7.203\,32\times10^{-4}$	$1.362\,96\times10^{-3}$

TABLE VI. Some values of the $2p$ subshell cross section σ (10^{-18} cm^2).

	Length		Velocity	
ω (eV)	Uncorrelated	Correlated	Uncorrelated	Correlated
111.9092	4.155 966	4.143 304	4.125 977	3.831 426
117.0114	4.390 768	3.915 401	4.327 141	3.993 270
132.9558	4.617 094	3.823 517	4.435 139	3.893 998
180.5761	3.478 000	2.960 488	3.153 742	2.962 858
234.1491	2.177 082	2.014 658	1.911 148	1.939 036
329.3899	0.960 941	1.017 209	0.862 118	0.944 308
451.8423	0.436 637	0.466 263	0.378 695	0.430 967
601.5064	0.193 132	0.209 859	0.170 643	0.196 387
778.3821	0.088 660	0.076 646	0.080 184	0.084 403
982.4695	0.042 602	0.040 053	0.039 4212	0.041 378

in the presence of two $1s$, two $2s$, six $2p$, and two $3s$ electrons.

The coupling scheme chosen for the excited states involving $2p$ correlations to the $3p$ subshell cross section was $2p^5\, kl(^1P)3s^2\, 3p\, ^{2S+1}L$, where kl represents a continuum orbital with energy $\frac{1}{2}k^2$ and angular momentum $l=0$ or 2. As shown by Amus'ya *et al.*,[14] this choice of potential for the excited states will cancel many otherwise large diagrams. This is discussed further in Sec. III C. For the excited states involving $3s$ correlations to the $3p$ subshell cross section, the coupling was $3s\, 3p(^{1,3}P)kp\, ^{2S+1}L$. Two sets of excited $l=1$ states were used, corresponding to a ^1P and ^3P core. These states are not strictly orthogonal to the $2p$ and $3p$ states, but the overlaps were small enough to be ignored.

The configuration $3s\, 3p^2$ lies below threshold, and correlations involving this configuration, such as Fig. 1(b) with $p=3p$, $k=ks$ or kd, $q=3s$, and $k'=3p$, were found to be important. Matrix elements involving $3s \rightarrow 3p$ transitions are an order of magnitude larger than those involving $3s \rightarrow np$ transitions with $n>3$. Figure 3 shows a comparison of our $3p$ subshell cross section (without resonances) to that of Chapman and Henry.[13]

Resonances in the $3p$ subshell cross section arise from the following intermediate states: $3s\, 3p\ (^{1,3}P)\, np\, ^2L$ ($n\geq 4$); $2p^5\, ns\ (^1P)\, 3s^2\, 3p\, ^2L$ ($n\geq 4$); and $2p^5\, nd\ (^1P)\, 3s^2\, 3p\, ^2L$ ($n\geq 3$), where $L=0$ and 2. Interactions between the $^1P\, np\, ^2L$ and $^3P\, np\, ^2L$ were included as in Sec. II. Also $2p^5\, ns\ (^1P)\, 3p\, ^2L$ and $2p^5\, nd\ (^1P)\, 3p\, ^2L$ series interactions were included. Resonances in the $3p \rightarrow kd$ cross section were much broader than in the $3p \rightarrow ks$ cross section. The cross section shown in Fig. 5 for $\omega < 22.88$ eV is due to the $3p$ subshell only. The very sharp spikes

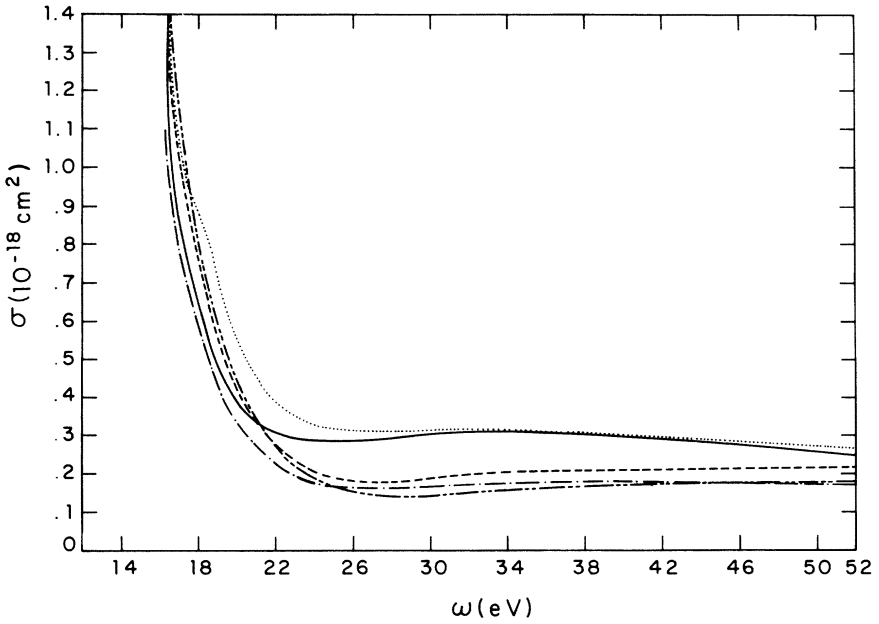

FIG. 3. Comparison of $3p$ cross sections near threshold. Dash line is length form, uncorrelated; solid line is length form including correlations with the $2p$ and $3s$ subshells; dash-dot line is velocity form, uncorrelated; dotted line is velocity form including correlations; dash-dash dot-dot line is $3p$ cross section of Ref. 13.

are resonances in the $3p \rightarrow ks$ cross section and extend upward to approximately 100 Mb. Resonances 1–5 of Fig. 5 are due to the intermediate states $(^3P)4p$, $(^3P)5p$, $(^1P)4p$, $(^3P)6p$, and $(^3P)7p$, respectively. Of course, there is actually an infinite number of resonances converging to the absorption edge; for legibility, only the first few resonances of any series are indicated on the figures. The largest energy shift in the position of the resonances is due to the $(^1P)4p$ resonance being embedded in the $(^3P)np$ series. The $(^1P)4p$ resonance repels the $(^3P)5p$ and $(^3P)6p$ resonances and increases their separation by approximately 1.0 eV.

B. 3s subshell cross section

The excitation of a 3s electron in Si II leads to $3s\,3p\ (^{1,3}P)\ kp\ ^2S$, ^2P, and ^2D final states. Two sets of continuum p orbitals were calculated, corresponding to the ^1P and ^3P core, and each averaged over the final coupling.

A cross section averaged over M_L was calculated for each of the ^2S, ^2P, and ^2D final-state couplings. The cross sections were then added to yield total cross sections for the ^1P and ^3P cores. The cross sections, without resonances, are shown in Fig. 4. The curve labeled 3 is the 3s subshell cross section leaving the residual Si III ion in a ^3P state; the curve labeled 4 is the 3s subshell cross section leaving the residual Si III ion in a ^1P state. The dip in the ^1P cross section around 100 eV is due to large correlation diagrams involving the 3p subshell which correlates primarily with terms involving the ^1P core.

Resonances in the $3s \rightarrow (^1P)\,kp\ ^2S$, ^2P, and ^2D cross sections arise from the states $2p^5\,nd\ (^1P)\ 3s^2\,3p\ ^2S$, ^2P, and $^2D\,(n \geq 3)$ and $2p^5\,ns\ (^1P)\ 3s^2\,3p\ ^2S$, ^2P, and $^2D\,(n \geq 4)$. For the 3s $(^3P)kp\ ^2S$, ^2P and ^2D cross sections, resonances arise not only from the 2p excitations mentioned above, but also from $3s\,3p\ (^1P)\ np\ ^2S$, ^2P, and $^2D\,(n \geq 5)$.

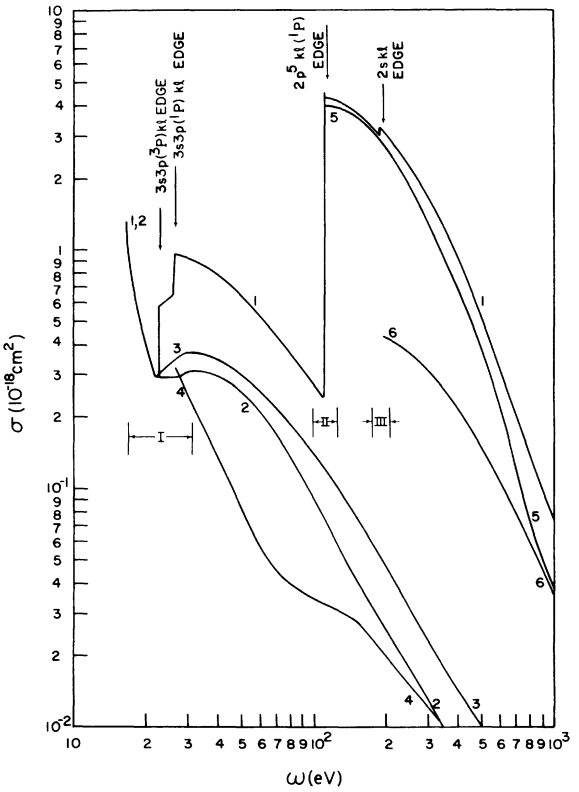

FIG. 4. Total and subshell cross sections without resonances (length form). (1) total cross section; (2) 3p subshell cross section; (3) 3s cross section leaving the residual Si III in a ^3P state; (4) 3s cross section leaving the residual Si III in a ^1P state; (5) the 2p cross section; and (6) the 2s cross section. I is the region of the $3s \rightarrow np$ resonances, shown in Fig. 5; II is the region of the $2p \rightarrow nl$ resonances, shown in Fig. 6; and III is the region of the $2s \rightarrow np$ resonances, shown in Fig. 7.

C. 2p and 2s subshell cross sections

The coupling schemes chosen for the excitation of a 2p electron from Si II were $2p^5\,k\ell(^1P)3s^2\,3p\ ^2S$, ^2P, and ^2D, where $\ell = 0,2$. Our single-particle potential cancels all matrix elements with passive, unexcited states and diagrams such as Fig. 1(b) and its exchange, where p and q both refer to the 2p orbital.[14,15] These diagrams can be large[15] and their cancellation by the potential takes a great burden off the perturbation expansion. The 2p nonresonance cross section is shown in Fig. 4 by the curve labeled 5.

Resonances occurring from $2s \rightarrow np$ excitations with $n \geq 3$ were included without any correlations in $Z(2s \rightarrow np)$. Figure 7 shows the $2s \rightarrow np$ resonances in the 2p cross section. The background in Fig. 7, however, is the total cross section, not merely the 2s cross section.

The 2s subshell cross section is included for the sake of completeness to 1 keV and is labeled curve 6 in Fig. 4. Only the lowest-order result is presented. No correlations were included, and Hartree-Fock single-particle energies were used.

D. Total cross section

The total cross section is the sum of the subshell cross sections, and is shown without resonances (in the length form) as the curve labeled 1 in Fig. 4. The behavior of the cross section in the region of the $3s \rightarrow np$ resonances is presented in Fig. 5. The resonance due to the state $3s\,3p\ (^3P)$ $4p\ ^2S$ and ^2D, lying between 17 and 19 eV, has a

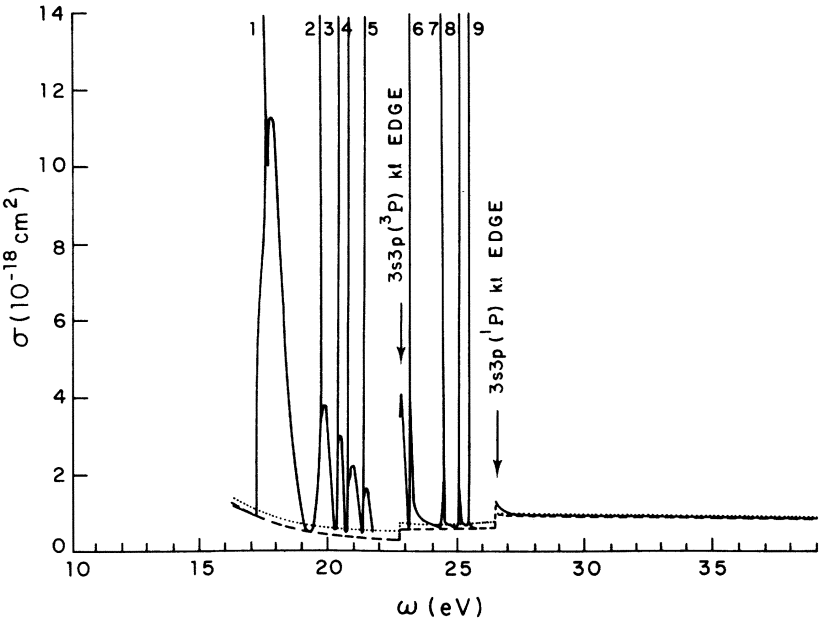

FIG. 5. Total cross section in region of $3s \rightarrow np$ resonances. Solid line is total cross section, length form; dotted line is correlated nonresonant velocity cross section; dash line is correlated nonresonant length cross section. The resonances are due to the following intermediate states: (1) $3s\,3p\,(^3P)4p\,^2S,^2D$; (2) $3s\,3p\,(^3P)5p\,^2S^2D$; (3) $3s\,3p\,(^1P)4p\,^2S$, ^2D; (4) $3s\,3p\,(^3P)6p\,^2S,^2D$; (5) $3s\,3p\,(^3P)7p\,^2S,^2D$; (6) $3s\,3p\,(^1P)5p\,^2S,^2D$; (7) $3s\,3p\,(^1P)6p\,^2S,^2D$; (8) $3s\,3p\,(^1P)7p\,^2S,^2D$; and (9) $3s\,3p\,(^1P)8p\,^2S,^2D$.

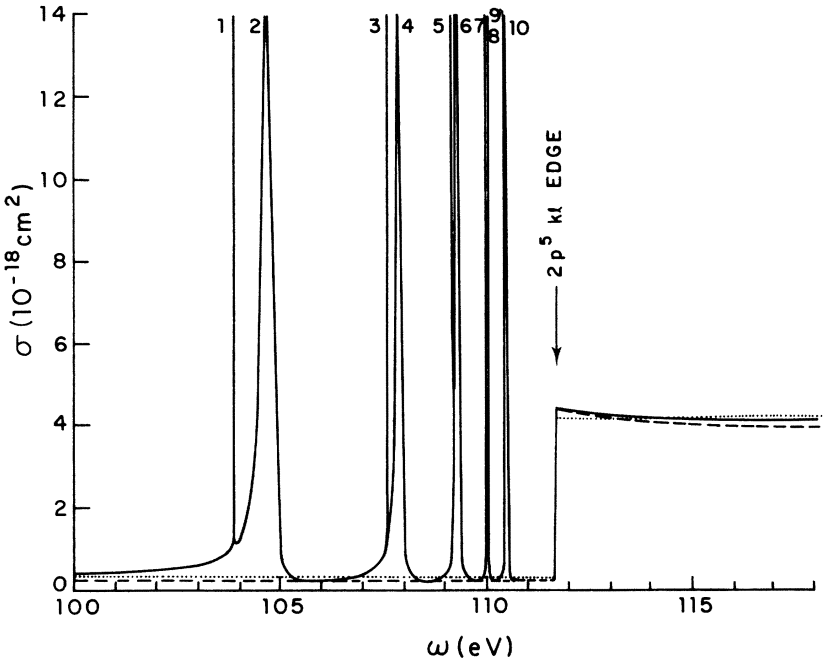

FIG. 6. Total cross section in region of $2p \rightarrow ns$ and nd resonances. Solid line is total cross section, length form; dotted line is correlated nonresonant velocity cross section; dash line is correlated nonresonant length cross section. The resonances are due to the following intermediate states: (1) $2p^5\,4s\,(^1P)3s^2\,3p\,^2S$, ^2P, ^2D; (2) $2p^5\,3d\,(^1P)3s^2\,3p\,^2S$, ^2P, ^2D; (3) $2p^5\,5s\,(^1P)3s^2\,3p\,^2S$, ^2P, ^2D; (4) $2p^5\,4d\,(^1P)3s^2\,3p\,^2S$, ^2P, ^2D; (5) $2p^5\,6s\,(^1P)3s^2\,3p\,^2S,^2P$, ^2D; (6) $2p^5\,5d\,(^1P)3s^2\,3p\,^2S$, ^2P, ^2D; (7) $2p^5\,7s\,(^1P)3s^2\,3p\,^2S$, ^2P, ^2D; (8) $2p^5\,6d\,(^1P)3s^2\,3p\,^2S$, ^2P, ^2D; (9) $2p^5\,8s\,(^1P)3s^2\,3p\,^2S$, ^2P, ^2D; (10) $2p^5\,7d$ $(^1P)3s^2\,3p\,^2S$, ^2P, ^2D.

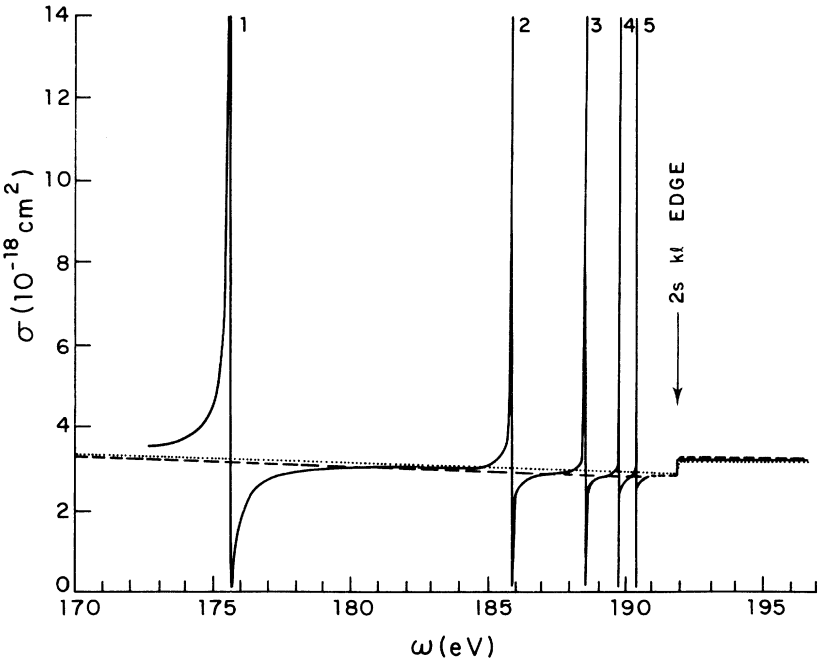

FIG. 7. Total cross section in region of $2s \rightarrow np$ resonances. Solid line is total cross section, length form; dotted line is correlated nonresonant velocity cross section; dash line is correlated nonresonant length cross section. The resonances are due to the following intermediate configurations: (1) $2s\,2p^6\,3s^2\,3p^2$; (2) $2s\,2p^6\,3s^2\,3p\,4p$; (3) $2s\,2p^6\,3s^2\,3p\,5p$; (4) $2s\,2p^6\,3s^2\,3p\,6p$; and (5) $2s\,2p^6\,3s^2\,3p\,7p$.

broad profile in the $3s^2\,kd\,^2D$ channel and a very narrow profile in the $3s^2\,ks\,^2S$ channel. The difference in position of the resonance peaks in the ks and kd cross sections is due to interacting resonance effects within the ks and kd cross sections.

The total cross section in the region of the $2p \rightarrow ns$, nd resonances is shown in Fig. 6. The extremely narrow spikes are due to $2p \rightarrow ns$ excitations, the broader peaks to $2p \rightarrow nd$ excitations. Resonances from the $2s \rightarrow np$ excitations are shown in Fig. 7. They were only included in the $2p$ subshell cross section. The shape of the resonances would be altered somewhat by including the $2s \rightarrow np$ resonances in the $3s$ and $3p$ subshell cross sections.

The resonance heights generally ranged from 500–1500 Mb, although the $2p \rightarrow ns$ resonances are much higher due to their extreme narrowness. Since the resonances have small half-widths relative to the separation between them, their interaction was generally small. The largest shift was due to the $3s\,3p\,(^1P)\,4p\,^2D$ being embedded in the $3s\,3p\,(^3P)\,np\,^2D$ series, as was discussed in Sec. III A. Shifts in the positions of the resonances due to interaction effects are less than 1 eV.

IV. CONCLUSIONS

We have shown how one may extract from the Brueckner-Goldstone perturbation expansion contributions to fully LS-coupled states by the use of projection operators. The results for this case are equivalent to those of the Rayleigh-Schrödinger perturbation expansion with multideterminant states. Using these methods, we have calculated the photoionization cross section of Si II from threshold to 1 keV, including effects from interacting resonances. The resonances are generally narrow and the interaction among them results in a shift in the resonance position of less than 1 eV.

Reasonable agreement between length and velocity forms of the cross section was obtained. However, the calculation of cross sections for LS-coupled states is found to affect the agreement quite markedly. As seen from Table VI, the ratio L/V of the correlated length and correlated velocity $2p$ cross sections ranges from 0.91 to 1.08. Tables IV and V for the $3s$ cross section, however, show that near threshold the ratio L/V for the ^3P core is 0.74 while for the ^1P core it is 1.33. Thus, while the two couplings show differences near threshold of approximately 30%, for the whole $3s$ subshell (the many-body result if we had not projected onto the ^1P and ^3P core states), the ratio L/V is 0.96. For the $3p$ subshell Table III shows that near threshold $L/V = 0.84$. Comparison of the uncorrelated length to velocity ratios with the correlated length to veloc-

ity ratios shows that, while adding correlations does improve the agreement between the two forms, it would be desirable to investigate higher-order diagrams.

Contributions due to photoionization accompanied by excitation were not included in this work. We hope to study this in later work.

ACKNOWLEDGMENTS

We wish to thank Professor C. F. Fischer, Dr. R. L. Chase, and Dr. J. H. Miller for the use of their computer programs in this work. We also thank Dr. R. L. Chase, Dr. J. J. Chang, and Dr. A. W. Fliflet for helpful discussions.

---

*Work supported by the National Science Foundation.

[1]C. Jordan, Astrophys. J. 156, 49 (1969).

[2]O. Engvold and Ö. Hauge, Nucl. Instrum. Methods 90, 351 (1970).

[3]V. P. Myerscough and G. Peach, in *Case Studies in Atomic Collision Physics II*, edited by E. W. McDaniel and M. R. C. McDowell (North-Holland, Amsterdam, 1972), p. 293.

[4]K. A. Brueckner, Phys. Rev. 97, 1353 (1955); *The Many-Body Problem* (Wiley, New York, 1959); J. Goldstone, Proc. Roy. Soc. A 239, 267 (1957).

[5]U. Fano, Phys. Rev. 124, 1866 (1961); U. Fano and J. W. Cooper, Rev. Mod. Phys. 40, 441 (1968).

[6]A. W. Fliflet and H. P. Kelly, Phys. Rev. A 10, 508 (1974).

[7]H. P. Kelly, Phys. Rev. 182, 84 (1969).

[8]H. P. Kelly and A. Ron, Phys. Rev. A 5, 168 (1972).

[9]H. P. Kelly, Phys. Rev. 136, B896 (1964).

[10]See, for example, H. A. Bethe and R. Jackiw, *Intermediate Quantum Mechanics* (Benjamin, New York, 1968), p. 201.

[11]S. L. Carter and H. P. Kelly (unpublished).

[12]H. P. Kelly, Phys. Rev. 131, 684 (1963).

[13]R. D. Chapman and R. J. W. Henry, Astrophys. J. 173, 243 (1972).

[14]M. Ya. Amus'ya, N. A. Cherepokov, and L. V. Chernysheva, Zh. Eksp. Teor. Fiz. 60, (1971) [Sov. Phys.—JETP 33, 90 (1971)].

[15]H. P. Kelly and R. L. Simons, Phys. Rev. Lett. 30, 529 (1973).

[16]C. E. Moore, *Atomic Energy Levels*, Natl. Bur. Std. Circ. No. 467 (U. S. GPO, Washington, D. C., 1949).

[17]K. Siegbahn, C. Nordling *et al.*, *ESCA* (Almqvist & Wiksells, Uppsala, 1967), p. 225.